

# Effects of dielectric mismatch and effective mass mismatch on exciton ground state energy in spherical Core/Shell nanostructures

A. IBRAL<sup>a,b</sup>, A. ZOUITINE<sup>c</sup>, S. AAZOU<sup>a,b</sup>, EL MAHDI ASSAID<sup>a,b\*</sup>, EL MUSTAPHA FEDDI<sup>c</sup>, F. DUJARDIN<sup>d</sup>

<sup>a</sup>*Equipe d'Optique et Electronique du Solide, Département de Physique, Faculté des Sciences, Université Chouaïb Doukkali, B. P. 20 El Jadida principale, El Jadida, Royaume du Maroc*

<sup>b</sup>*Laboratoire d'Instrumentation, Mesure et Contrôle, Département de Physique, Université Chouaïb Doukkali, B. P. 20 El Jadida principale, El Jadida, Royaume du Maroc*

<sup>c</sup>*Département de Physique, Ecole Nationale Supérieure d'Enseignement Technique, Université Mohammed V Souissi, B. P. 6207 Rabat-Instituts, Rabat, Royaume du Maroc*

<sup>d</sup>*LCPMC, Institut de Chimie, Physique et Matériaux, Université de Lorraine, 1 Bd Arago, 57070 Metz, France*

---

Exciton confined in a spherical core/shell nanostructure is studied in the framework of the envelope function approximation. Finite height barriers are used to describe conduction and valence band offsets between core and shell of the structure. Electron and hole effective masses mismatch between core and shell and dielectric mismatch at the surface where core and shell materials meet are taken into account. Exciton ground state energy is determined via the Ritz variational principle using a trial wave function where the coulomb attraction between electron and hole is considered. The theoretical approach developed is applied to determine the coulomb correlation parameter, the binding energy and the spatial extension of a bound electron-hole pair as functions of the core to shell radii ratio for CdS/HgS core/shell nanostructures immersed in aqueous or organic solution.

(Received September 2, 2013; accepted November 7, 2013)

*Keywords:* Exciton, Core/Shell nanostructure, Quantum dot, Dielectric mismatch

---

## 1. Introduction

Since the pioneering works done by Alexei I. Ekimov [1] and Louis E. Brus [2, 3] where quantum size effects have been reported for the first time, quantum dots have been studied extensively both experimentally and theoretically. Quantum dots are semiconductor droplets which may be precipitated by annealing in a semiconducting or in an isolating host matrix, or chemically synthesized at low temperature in colloidal organic solutions. Quantum dots are exotic structures which are intermediate between solids and atoms. They present the compactness of solids, but their electronic and optical properties are close to those of isolated atoms. Indeed, due to three-dimensional confinement, the degrees of freedom of charge carriers are frozen in all directions of space. Because of their nanometer scale size, the quantum characters of electrons and holes are revealed, their energies are quantized and depend on the dot size. Accordingly, the line corresponding to HOMO-LUMO transition is blue shifted. This property is known in the literature under the name of 'band gap engineering'.

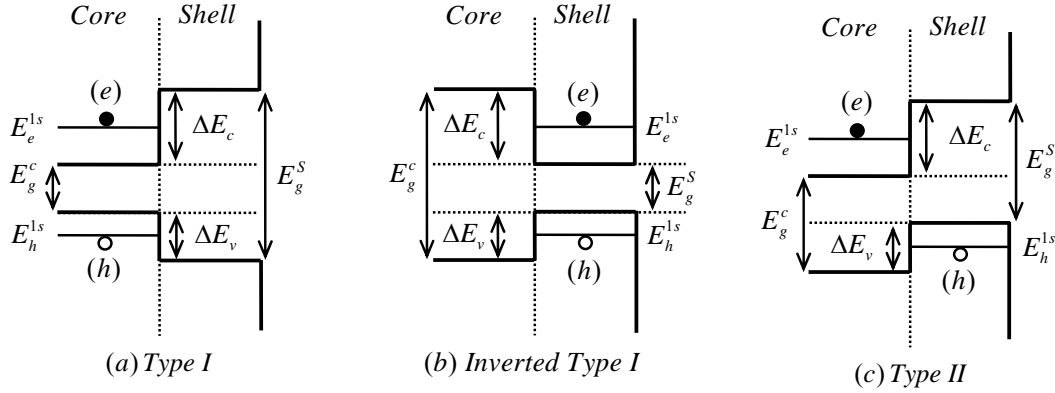
Nowadays, the experimental techniques of growth have made it possible to fabricate high-quality semiconductor quantum dots within a large range of sizes for different fields of applications such as optical encoding [4], multiplexing [5], energy harvesting [6], biology and

medicine where quantum dots are used in the study of intracellular processes at the single molecule level [7,8]. They are also used in high-resolution cellular imaging [9-12], in long term in vivo observation of cell trafficking, in tumor targeting and in diagnostics [13-16].

In the last decade, interest in quantum dots has partially shifted to core/shell nanostructures. These onion-like structures also named Quantum Dot Quantum Well structures [17] are mainly obtained via chemical processes of growth by capping a spherical quantum dot of a given semiconductor with a spherical shell of another semiconductor. This shell may also be coated by a spherical organic or inorganic thin layer to passivate quantum dot surface and to deactivate dangling bonds. According to band offsets between semiconductors involved, the final nanostructure may be of type I when electrons and holes are confined in the nanostructure core (CdSe/CdS [18], CdSe/ZnSe [19]) (see figure 1a), inverted type I when electrons and holes are confined in the nanostructure shell (CdS/CdSe [20], ZnSe/CdSe [21]) (see figure 1b), type II when electrons and holes are confined respectively in the core and the shell of the quantum dot (CdTe/CdSe [22], CdS/ZnSe [23]) or vice versa (see figure 1c). In core/shell nanostructures, electron and hole ground state energies as well as their probability densities may be tuned in advance which is known in the literature under the name of 'wave function engineering'.

According to the present state of the art, solution processable semiconducting colloidal core/shell nanostructures exhibit interesting optical properties. Their photoluminescence spectrum depends on semiconductors involved and also on core size and shell thickness. This

allows the synthesis of quantum dot size-tunable color colloidal solution, the fabrication of electrically driven colloidal quantum dot light emitting devices (QD-LED) and electrically driven full-color QD-LED displays [24].



Figs. 1. Conduction and valence band offsets for Type I (a), Inverted type I (b) and Type II (c) spherical core/shell nanostructures.

In this study, we focus on an inverted type I core/shell nanostructure (see figure 1b). First, we determine the single particles ground state energies and wave functions. We show that for a fixed dot radius  $R_s$ , the nanostructure is of inverted type I for a core radius lighter than a critical value  $R_{C1}$  (electron and hole are in the shell), of quasi type II for a core radius lying between two critical values  $R_{C1}$  and  $R_{C2}$  (electron is in the core and hole is in the shell or vice versa) and is of quasi type I for a core radius greater than a critical value  $R_{C2}$  (electron and hole are in the core). On the basis of the single particles wave functions, we construct a trial wave function for the bound electron-hole pair which takes into account the attractive coulomb correlation. Then, we determine via the Ritz variational principle the binding energy, the coulomb correlation parameter and the distance between particles of an exciton confined in a core/shell nanostructure for weak, intermediate and strong confinement regimes.

## 2. Theory

Let us consider an inverted type I core/shell hetero-nanostructure (see figure 1b). This kind of structure is composed by a spherical wide band gap semiconductor nanocrystal of radius  $R_c$  and a dielectric constant  $\epsilon_1$  playing the role of core, over coated with a narrower band gap semiconductor layer of a radius  $R_s$ , a thickness  $T = R_s - R_c$  and a dielectric constant  $\epsilon_2$  playing the role of a shell. The whole nanostructure is immersed in an aqueous or in an organic solution with a dielectric constant  $\epsilon_3$ . The bottom of core conduction band is above the bottom of shell conduction band (see figure 1b). The top of core valence band is below the top of shell valence band

(see Fig. 1b). Due to this well-like band profiles, electron and hole are partially confined in the narrowest band gap semiconductor.

### 2.1 Electron and hole ground state energies and wave functions:

In the framework of the effective mass approximation and assuming isotropic, parabolic and non-degenerated bands, the Hamiltonian  $H_i$  of a single particle, in CGS electrostatic units, reads:

$$H_i = \left( \frac{\hbar}{j} \nabla_i \right) \frac{1}{2m_i^*(r_i)} \left( \frac{\hbar}{j} \nabla_i \right) + V_{wi}(r_i) \quad (i = e, h) \quad (1)$$

where  $e$  and  $h$  refer, respectively, to a single electron and a single hole. In equation (1), the first term stands for the hermitian kinetic energy operator for a position dependent effective mass particle proposed for the first time by BenDaniel and Duke [25].

The electron and hole effective masses in unit of free electron mass  $m_0$  are given by:

$$m_i^*(r_i) = \begin{cases} m_{i1}^*, & r_i < R_c \\ m_{i2}^*, & R_c < r_i < R_s \end{cases} \quad (i = e, h) \quad (2)$$

$R_c$  and  $R_s$  are respectively inner and outer radii of the core/shell nanostructure (see Fig. 2).

The electron and hole confining potentials inside the narrowest band gap semi-conductor due to nanostructure band offsets between core, shell and host medium  $V_{wi}(r_i)$  ( $i = e, h$ ) are expressed as follows:

$$V_{wi}(r_i) = \begin{cases} V_{0i}, & 0 < r_i < R_C \\ 0, & R_C < r_i < R_S \\ \infty, & R_S < r_i \end{cases} \quad (i = e, h) \quad (3)$$

The Schrödinger equation giving single particles eigenvalues  $E_i$  and eigenfunctions  $\Psi_i(\vec{r}_i)$  writes:

$$H_i \Psi_i(\vec{r}_i) = E_i \Psi_i(\vec{r}_i) \quad (i = e, h) \quad (4)$$

The separation of radial and angular variables in equation (4) leads to the following expression of wave functions:

$$\Psi_i(\vec{r}_i) = R_i^{n,l}(r_i) Y_{l,m}(\theta, \varphi) \quad (i = e, h) \quad (5)$$

$R_i^{n,l}(r_i)$  ( $i = e, h$ ) are the radial part of wave functions,  $Y_{l,m}(\theta, \varphi)$  is a spherical harmonic,  $n$  is the principal quantum number,  $l$  and  $m$  are orbital and magnetic quantum numbers.

Afterwards, we focus on single particles ground states corresponding to the following quantum numbers  $n=1$ ,  $l=0$  and  $m=0$ , namely 1s states since the nanostructure effective gap is related to the shell semiconductor gap by the following equation:

$$E_g^{Core/Shell} = E_g^{Shell} + E_e^{1s} + E_h^{1s} \quad (6)$$

To determine the radial part  $R_i^{1s}(r_i)$  of a single particle wave function for all values of core radius  $R_C$  lying between 0 and a predetermined shell size  $R_S$ , one must consider two different cases. In the first one, single particle energy  $E_i^{1s} < V_{0i}$  and core radius  $R_C < R_{Ci}$  where  $R_{Ci}$  is a critical value of  $R_C$  corresponding to  $E_i^{1s} = V_{0i}$ . The maximum of probability density function is in the shell and the radial part  $R_i^{1s}(r_i)$  of single particle wave function writes:

$$R_i^{1s}(r_i) = \begin{cases} A_{1i} \frac{sh(k_{1i}r_i)}{r_i}, & 0 < r_i < R_C \\ A_{2i} \frac{\sin(k_{2i}(r_i - R_S))}{r_i}, & R_C < r_i < R_S \end{cases} \quad (i = e, h) \quad (7)$$

where  $k_{1i} = \sqrt{2m_{1i}(V_{0i} - E_i)/\hbar^2}$  and  $k_{2i} = \sqrt{2m_{2i}E_i/\hbar^2}$ . In the second case,  $E_i^{1s} > V_{0i}$  and  $R > R_{Ci}$ . The maximum of probability density function is in the core and the radial part  $R_i^{1s}(r_i)$  of single particle wave function reads:

$$R_i^{1s}(r_i) = \begin{cases} A_{3i} \frac{\sin(k_{3i}r_i)}{r_i}, & 0 < r_i < R_C \\ A_{4i} \frac{\sin(k_{4i}(r_i - R_S))}{r_i}, & R_C < r_i < R_S \end{cases} \quad (i = e, h) \quad (8)$$

where  $k_{3i} = \sqrt{2m_{1i}(E_i - V_{0i})/\hbar^2}$  and  $k_{4i} = \sqrt{2m_{2i}E_i/\hbar^2}$ .

In each case, the coefficients  $A_{ji}$  are determined via the normalization condition:

$$\int_0^{R_S} (R_i^{1s}(r_i))^2 4\pi r_i^2 dr_i = 1 \quad (9)$$

and the continuity condition of radial part of wave function  $R_i^{1s}(r_i)$  at core surface ( $r_i = R_C$ ):

$$R_{Core,i}^{1s}(r_i)_{r_i=R_C} = R_{Shell,i}^{1s}(r_i)_{r_i=R_C} \quad (10)$$

The ground state energies  $E_i^{1s}$  ( $i = e, h$ ) are determined after solving numerically the transcendental equations obtained by combining continuity conditions of radial part of wave function  $R_i^{1s}(r_i)$  and probability current density at core surface ( $r_i = R_C$ ):

$$\left. \frac{1}{m_{1i}} \frac{dR_{Core,i}^{1s}(r_i)}{dr_i} \right)_{r_i=R_C} = \left. \frac{1}{m_{2i}} \frac{dR_{Shell,i}^{1s}(r_i)}{dr_i} \right)_{r_i=R_C} \quad (11)$$

For a given value  $R_S$  of nanostructure size, the transcendental equations, giving the critical values of core radius  $R_{C,i}$  for which  $E_i^{1s} = V_{0i}$  ( $i = e, h$ ), are given by:

$$\left( R_C \sqrt{2m_{2i}V_{0i}/\hbar^2} \cot((R_C - R_S) \sqrt{2m_{2i}V_{0i}/\hbar^2}) \right)_{i=e,h} - 1 = 0 \quad (12)$$

## 2.2 Exciton ground state energy and wave function:

In CGS electrostatic units and under the same assumptions as for single particles, the Hamiltonian of a confined exciton writes :

$$H_x = -\frac{\hbar^2 \Delta_e}{2m_e^*(r_e)} - \frac{\hbar^2 \Delta_h}{2m_h^*(r_h)} + V_{we}(r_e) + V_{wh}(r_h) - \frac{e^2}{\varepsilon(r_e, r_h) r_{eh}} \quad (13)$$

$e$  is the elementary charge. The electron and hole positions dependent dielectric constant  $\varepsilon(r_e, r_h)$  reads:

$$\varepsilon(r_e, r_h) = \begin{cases} \varepsilon_1, & r_e < R_C \text{ and } r_h < R_C \\ \varepsilon_2, & R_C < r_e < R_S \text{ and } R_C < r_h < R_S \\ (\varepsilon_1 + \varepsilon_2)/2 & \text{otherwise} \end{cases} \quad (14)$$

The ground state of a confined exciton presents spherical symmetry. Thus, the corresponding wave function must be expressed in Hylleraas coordinates  $r_e, r_h$

and  $r_{eh}$ . Within these coordinates, the Laplacian operator writes:

$$\Delta_i = \frac{\partial^2}{\partial r_i^2} + \frac{2}{r_i} \frac{\partial}{\partial r_i} + \frac{r_i^2 - r_j^2 + r_{eh}^2}{r_i r_{eh}} \frac{\partial^2}{\partial r_i \partial r_{eh}} + \frac{\partial^2}{\partial r_{eh}^2} + \frac{2}{r_{eh}} \frac{\partial}{\partial r_{eh}} \quad (15)$$

where  $i, j = e, h$  ( $i \neq j$ ). The exciton ground state energy and the associated wave function are solutions of the effective Schrödinger equation:

$$H_X \Psi_X(r_e, r_h, r_{eh}) = E_X \Psi_X(r_e, r_h, r_{eh}) \quad (16)$$

This equation is not solvable analytically, so we have to determine its ground state solutions using an approximation method. Here, we use the Ritz variational principle. We choose the following trial wave function:

$$\Psi_X(r_e, r_h, r_{eh}) = R_{0,0}^e(r_e) R_{0,0}^h(r_h) \exp(-\alpha r_{eh}) \quad (17)$$

$R_{0,0}^e(r_e)$  and  $R_{0,0}^h(r_h)$  are, respectively, the electron and hole wave functions given in section 2.1. The exponential factor is introduced in order to take into account the coulomb attraction between electron and hole.  $\alpha$  is a variational parameter. The exciton ground state energy  $E_X$  is obtained by minimization of the expectation value of  $H_X$  with respect to  $\alpha$ :

$$E_X = \min_{\alpha} \frac{\langle \Psi_X | H_X | \Psi_X \rangle}{\langle \Psi_X | \Psi_X \rangle} \quad (18)$$

The exciton binding energy  $E_b$  is expressed as follows:

$$E_b = E_e^{1s} + E_h^{1s} - E_X \quad (19)$$

In this study we focus on CdS/HgS core/shell nanostructures where, for predetermined value of shell radius  $R_S$ , critical value of core radius  $R_{Ch}$  corresponding to hole energy  $E_h^{1s}$  equal to valence band offset  $\Delta E_v$  is lighter than critical value of core radius  $R_{Ce}$  corresponding to electron energy  $E_e^{1s}$  equal to conduction band offset  $\Delta E_c$ . Accordingly, for core radius  $R < R_{Ch}$ ,  $E_h^{1s} < \Delta E_v$  and  $E_e^{1s} < \Delta E_c$ , electron, hole and bound electron-hole pair are confined in shell of nanostructure (see figure 2.1), both  $R_{0,0}^e(r_e)$  and  $R_{0,0}^h(r_h)$  are given by equation (7). For core radius lying between  $R_{Ch}$  and  $R_{Ce}$ ,  $E_h^{1s} > \Delta E_v$  and  $E_e^{1s} < \Delta E_c$ , hole is confined in the whole structure and electron is still confined in its shell (see figure 2.2). As a result, bound electron-hole pair is spatially separated,  $R_{0,0}^e(r_e)$  is given by equation (7) while  $R_{0,0}^h(r_h)$  is given by equation (8). Finally, for core radius lying between  $R_{Ce}$  and  $R_S$ ,  $E_h^{1s} > \Delta E_v$  and  $E_e^{1s} > \Delta E_c$ , electron, hole and bound electron-hole pair are confined in the whole structure (see figure 2.3),  $R_{0,0}^e(r_e)$  and  $R_{0,0}^h(r_h)$  are given by equation (8).

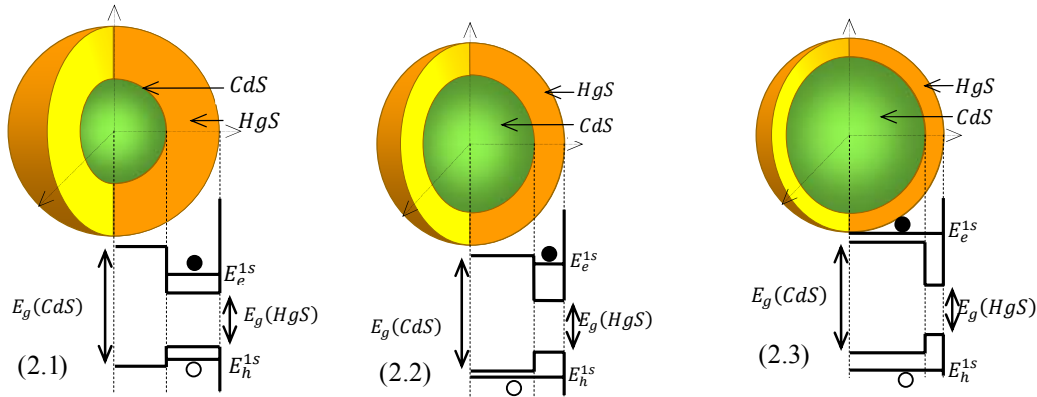


Fig. 2. Inverted type I CdS/HgS core/shell nanostructures with different electron-hole spatial correlations : (2.1) both electron and hole are in the shell, (2.2) hole is in the core and electron is in the shell, (2.3) both electron and hole are in the core.

### 3. Results and discussion

To lighten single particles Hamiltonians (equation 1) and exciton Hamiltonian (equation 13), we use as unit of length  $a_x^* = \bar{\epsilon} \hbar^2 / e^2 \bar{\mu} = 4.9779 \text{ nm}$ , which represents light hole-exciton effective Bohr radius of an intermediate bulk material between CdS and HgS (see Table 1). We use as

unit of energy  $R_x^* = \bar{\mu} e^4 / 2 \bar{\epsilon}^2 \hbar^2 = 17.1513 \text{ meV}$ , which represents absolute value of light hole-exciton ground state energy in the intermediate bulk material between CdS and HgS (see Table 1).  $\bar{\epsilon} = (\epsilon_1 + \epsilon_2) / 2$  is the mean relative dielectric constant.  $\bar{\mu} = \overline{m_e^* m_h^*} / (m_e^* + m_h^*)$  is the reduced mass of exciton in the intermediate bulk material.

$\overline{m}_i^* = (\overline{m}_{i1}^* + \overline{m}_{i2}^*)/2$  ( $i = e, h$ ) are single particles mean effective masses.

Table 1. CdS and HgS physical parameters used in the numerical calculations.

	CdS	HgS	Intermediate bulk material
$m_e^* / m_0$	0.2 [17]	0.036 [17]	0.118
$m_h^* / m_0$	0.7 [17]	0.044 [17]	0.372
$\mu$	0.1555	0.0198	0.0895
$E_g$ (eV)	2.5 [17]	0.5 [17]	-
$\varepsilon / \varepsilon_0$	5.5 [17]	11.36 [17]	8.43
$a_x^*$ (nm)	1.8716	30.3610	4.9779
$R_x^*$ (meV)	69.9405	2.0875	17.1513

In what follows, we will investigate the effects of : i) finite band offsets  $\Delta E_c$  and  $\Delta E_v$  between core and shell, ii) effective mass mismatch at the boundary between core and shell, iii) dielectric mismatch between core and shell materials on variational parameter  $\alpha$ , binding energy  $E_b$  and spatial extension  $\langle r_{eh} \rangle$  of an exciton confined in a CdS/HgS core/shell nanostructure [26], [27].

In figures (3.1), (3.2) and (3.3), the variations of coulomb correlation parameter  $\alpha$ , binding energy  $E_b$  and inter-particle distance  $\langle r_{eh} \rangle$  are drawn against core to shell radii ratio  $R_c / R_s$  for a shell radius  $R_s = 4$  ex. units. Numerical calculations are performed according four different models. In the first one, confinement inside shell is modeled by an infinitely deep potential well and effects of effective mass mismatch and dielectric mismatch are neglected (cyan lines labeled (a)). In the second model, conduction and valence band offsets  $\Delta E_c$  and  $\Delta E_v$  between core and shell are modeled by finite height barriers and their effect is examined (blue lines labeled (b)). In the third model, effects of electron and hole effective masses mismatch are added (green lines labeled (c)). Finally, ultimate effect of dielectric mismatch between core and shell materials is added in the last model (red lines labeled (d)).

In case of infinite band offsets between core and shell, exciton is completely confined in shell. For an inner to outer radii ratio  $R_c / R_s \rightarrow 0$ , core/shell nanostructure reduces to a spherical quantum dot,  $\alpha \rightarrow 0.845$  ex. units,  $E_b \rightarrow 1.365$  ex. units and  $\langle r_{eh} \rangle \rightarrow 1.368$  ex. units. These limit values are in good agreement with the results obtained by El Khamkhami *et al.* [28] and by Kayanuma [29]. For an inner to outer radii ratio  $R_c / R_s \rightarrow 1$ , exciton which is completely confined in nanostructure shell has a bi-dimensional character,  $\alpha \rightarrow 2$  ex. units,  $E_b \rightarrow 4$  ex. units and  $\langle r_{eh} \rangle \rightarrow 0.5$  ex. units. These limit values are consistent with those found in the literature [28], [30].

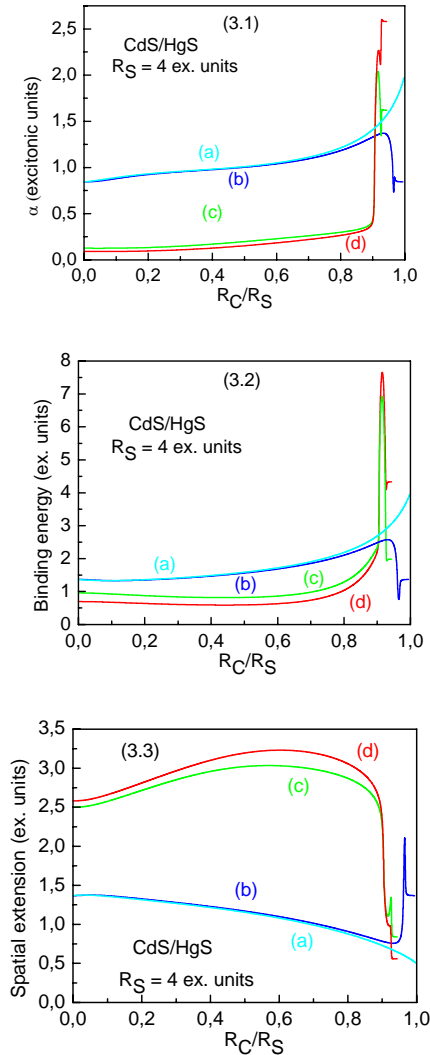


Fig. 3: Variational parameter  $\alpha$  (3.1), binding energy  $E_b$  (3.2) and spatial extension  $\langle r_{eh} \rangle$  (3.3) versus core to shell radii ratio  $R_c / R_s$  of an exciton confined in a CdS/HgS core/shell nanostructure with a shell radius  $R_s = 4$  ex. units.

In case of finite band offsets between CdS and HgS, leakage of exciton wave function toward core region is no more negligible especially for thin HgS layer. For  $R_C/R_S \rightarrow 0$ , core/shell nanostructure reduces to a spherical QD. When  $R_C/R_S$  increases, we have competition between tridimensional confinement in a quantum dot and bidimensionnal confinement in a quantum well, exciton binding energy decreases. For a critical value  $(R_C/R_S)_{crit}^{finite}$ , exciton binding energy is minimal. When  $R_C/R_S$  is lying between  $(R_C/R_S)_{crit}^{finite}$  and  $(R_C/R_S)_{2D}$ , exciton binding energy increases. For a value of the ratio  $R_C/R_S$  equal to  $(R_C/R_S)_{2D}$ , both electron and hole are confined in a thin HgS layer, their interparticle distance is minimal. Exciton presents the most pronounced bidimensional character, its coulomb correlation parameter and binding energy are maximal. When  $R_C/R_S$  increases from  $(R_C/R_S)_{2D}$  to  $R_{ch}/R_S$ , exciton binding energy decreases due to hole relaxation in core. For  $R_C/R_S$  equal to  $R_{ch}/R_S$ , hole is no more confined in the HgS layer and oscillatory part of its wave function is extended over the entire structure. For a structure such as  $R_{ch} \leq R_C \leq R_{ce}$ , oscillatory part of hole wave function is extended over the whole structure while oscillatory part of electron wave function is localized in HgS layer, bound electron-hole pair is spatially separated and interparticle distance is maximal. Exciton behaves like a non-correlated electron-hole pair, its coulomb correlation parameter and binding energy are minimal. When  $R_C/R_S$  is equal to  $R_{ce}/R_S$ , electron is no more confined in HgS layer and oscillatory part of its wave function is extended over the entire structure. For a structure such as  $R_{ce}/R_S < R_C/R_S < 1$ , exciton binding energy increases. When  $R_C/R_S \rightarrow 1$ , core/shell nanostructure reduces to a spherical QD.

In case where effects of electron and hole effective masses mismatch are taken into account, and in ultimate case where effects of dielectric mismatch between core and shell materials are considered, the plots of coulomb correlation parameter  $\alpha$ , binding energy  $E_b$  and interparticle distance  $\langle r_{eh} \rangle$  present the same shape as for the second case. A careful study of exciton asymptotic behavior for large dots allows us to say that in third case, when  $R_C/R_S \rightarrow 0$ ,  $E_b \rightarrow 0.956$  ex. units, and when  $R_C/R_S \rightarrow 1$ ,  $E_b \rightarrow 1.983$  ex. units. While in ultimate case, when  $R_C/R_S \rightarrow 0$ ,  $E_b \rightarrow 0.696$  ex. units, and when  $R_C/R_S \rightarrow 1$ ,  $E_b \rightarrow 4.332$  ex. units. The most important thing that must be reported is that in the two latter cases, we assist to a giant electron-hole coulomb correlation that enhances exciton binding energy up to 7.655 ex. units (131 meV) for a 0.34 ex. units (1.68 nm) thick HgS layer which corresponds to three HgS atomic layers [17].

In Figs. (4.1), (4.2) and (4.3), variations of coulomb correlation parameter  $\alpha$ , binding energy  $E_b$  and interparticle distance  $\langle r_{eh} \rangle$  are plotted versus core to shell radii ratio  $R_C/R_S$  for weak confinement regime  $R_S = 4$  ex. units (orange lines), intermediate confinement regime  $R_S = 2$  ex. units (blue lines), strong confinement regime  $R_S = 1$  (green lines) and 0.8 ex. units (red lines). Numerical calculations are performed according the most sophisticated model which takes into account all effects involved.

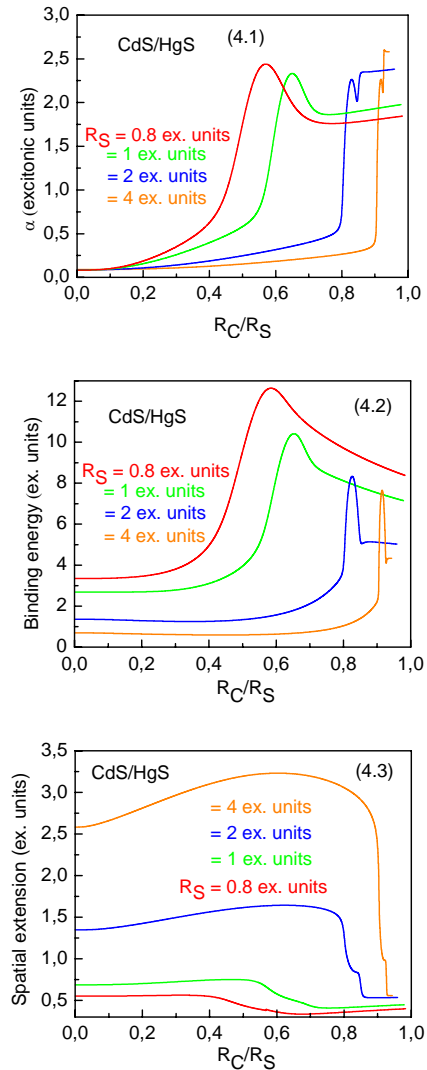


Fig. 4: Variational parameter  $\alpha$  (4.1), binding energy  $E_b$  (4.2) and spatial extension  $\langle r_{eh} \rangle$  (4.3) against core to shell radii ratio  $R_C/R_S$  of an exciton confined in a CdS/HgS core/shell nanostructure for weak confinement regime  $R_S = 4$  ex. units, intermediate confinement regime  $R_S = 2$  ex. units and strong confinement regime  $R_S = 1$  and 0.8 ex. units.

The three curves show clearly the competition between tridimensional confinement in spherical semiconductor quantum dot and bidimensionnal confinement in spherical thin HgS layer. Indeed, when  $R_C/R_S \rightarrow 0$ , core/shell nanostructure is equivalent to spherical HgS quantum dot. When  $R_C/R_S \rightarrow 1$ , core/shell nanostructure is comparable to spherical CdS quantum dot. However, for a 0.3 to 0.4 thick HgS layer, core/shell nanostructure behaves like an HgS quantum well.

#### 4. Conclusion

To summarize, in the framework of the envelope function approximation, we determined analytically the

ground state energies and wave functions of an electron and a hole confined in a CdS/HgS core/shell nanostructure, as functions of the inner to outer radii ratio. We showed that electron (hole) energy increase (decrease) monotonously when core radius increases from 0 to shell radius. Thus, it is possible to fabricate nanostructures with an effective band gap engineered in advance. Using the Ritz variational principle, we determined the ground state energy and the wave function of an exciton confined in a core/shell nanostructure. According to core to shell radii ratio, we highlighted three styles of geometric confinement where exciton is confined in core, in shell or spatially separated. We also determined coulomb correlation parameter, binding energy and spatial extension of the confined exciton against the inner to outer radii ratio. We showed that for nanostructures such as the thickness of spherical HgS layer is about 1.7 nm, we assist to a giant electron-hole coulomb correlation that enhances exciton binding energy up to ten times the binding energy in HgS spherical quantum dots.

#### Acknowledgments

Asmaa IBRAL is grateful to CNRST of Morocco for its financial support under grant N° G12/003.

#### References

- [1] A. I. Ekimov and A. A. Onushchenko, Pis'ma. Zh. Eksp. Teor. Fiz, **34**(6), 363 (1981).
- [2] L. E. Brus, J. Chem. Phys. **79**, 5566 (1983).
- [3] L. E. Brus, J. Chem. Phys. **80**(9), 4403 (1984).
- [4] Zhenda Lu, Chuanbo Gao, Qiao Zhang, Miaofang Chi, Jane Y. Howe, Yadong Yin, Nano Lett. **11**(8), 3404 (2011).
- [5] W. Russ Algar, Mario G. Ancona, Anthony P. Malanoski, Kimihiro Susumu, Igor L. Medintz, ACS Nano, **6**(12), 11044 (2012).
- [6] Roberto Trevisan, Pau Rodenas, Victoria Gonzalez-Pedro, Cornelia Sima, Rafael Sánchez Sánchez, Eva M. Barea, Ivan Mora-Sero, Francisco Fabregat-Santiago, Sixto Gimenez, J. Phys. Chem. Lett., **4**(1), 141 (2013).
- [7] Jui-Ming Yang, Haw Yang and Liwei Lin, ACS Nano, **5**(6), 5067 (2011).
- [8] Igor L. Medintz, Thomas Pons, James B. Delehanty, Kimihiro Susumu, Florence M. Brunel, Philip E. Dawson and Hedi Mattoussi, Bioconjugate Chem, **19**(9), 1785 (2008).
- [9] Jianbo Liu, Xiaohai Yang, Kemin Wang, Yan He, Pengfei Zhang, Haining Ji, Lixin Jian, Wei Liu, Langmuir, **28**(28), 10602 (2012).
- [10] Patrick Hoyer, Thorsten Staudt, Johann Engelhardt, Stefan W. Hell, Nano Lett., **11**(1), 245 (2011).
- [11] Shawn J. Tan, Nikhil R. Jana, Shujun Gao, Pranab K. Patra and Jackie Y. Ying, Chem. Mater., **22**(7), 2239 (2010).
- [12] Simon Hennig, Sebastian van de Linde, Mike Heilemann, Markus Sauer, Nano Lett., **9**(6), 2466 (2009).
- [13] Christina Tekle, Bo van Deurs, Kirsten Sandvig, Tore-Geir Iversen, Nano Lett., **8**(7), 1858 (2008).
- [14] Sujata Sundara Rajan, Hong Yan Liu, Tania Q. Vu, ACS Nano, **2**(6), 1153 (2008).
- [15] Vasudevanpillai Biju, Damodaran Muraleedharan, Ken-ichi Nakayama, Yasuo Shinohara, Tamitake Itoh, Yoshinobu Baba and Mitsuru Ishikawa, Langmuir, **23**(20), 10254 (2007).
- [16] Sébastien Courty, Camilla Luccardini, Yohanns Bellaiche, Giovanni Cappello, Maxime Dahan, Nano Lett., **6**(7), 1491 (2006).
- [17] D. Schooss, A. Mews, A. Eychmüller, H. Weller, Phys. Rev. B **49**(24), 17072 (1994).
- [18] M. Marceddu, M. Saba, F. Quochi, A. Lai, J. Huang, D. V. Talapin, A. Mura, G. Bongiovanni, Nanotechnology **23**, 15201 (2012).
- [19] S. Rawalekar, M. V. Nikhil Raj, H. N. Ghosh, Science of Advanced Materials, **4**(5-6), 637(6) (2012).
- [20] Z. Pan, H. Zhang, K. Cheng, Y. Hou, J. Hua, X. Zhong, ACS Nano, **6**(5), 3982 (2012).
- [21] L. P. Balet, S. A. Ivanov, A. Piryatinski, M. Achermann, V. I. Klimov, Nano Letters, **4**(8), 1485 (2004).
- [22] S. A. Ivanov, A. Piryatinski, J. Nanda, S. Tretiak, K. R. Zavadil, W. O. Wallace, D. Werder, V. I. Klimov, J. Am. Chem. Soc., **129**, 11708 (2007).
- [23] M. Schmidt, M. Grün, S. Petillon, E. Kurtz, C. Klingshirn, Appl. Phys. Lett. **77**, 85 (2000).
- [24] Y. Shirasaki, G. J. Supran, M. G. Bawendi, V. Bulović, Nature photonics, **7**, 13 (2013).
- [25] D. J. BenDaniel, C. B. Duke, Physical Review **152**(2), 683 (1966).
- [26] Asmaa Ibral, Safae Aazou, El Mahdi Assaid, El Mustapha Feddi, Francis Dujardin, M'Hamed El Aydi, Proceedings of the First International Conference on Advanced Materials for Photonics, Sensing and Energy Conversion Applications, El Jadida, Morocco, 5-7 December 2013, p. 176.
- [27] Asmaa Ibral, Asmaa Zouitine, Safae Aazou, El Mahdi Assaid, El Mustapha Feddi, Francis Dujardin, and M'Hamed El Aydi, Proceedings of the Fourth International Meeting on Dielectric Materials. Marrakech, Morocco, 29-31 May 2013, p. 39.
- [28] J. El Khamkhami, E. Feddi, E. Assaid, F. Dujardin, B. Stébé, J. Diouri, Physica E **15**, 99 (2002).
- [29] Y. Kayanuma, Phys. Rev. B **38**(14), 9797 (1988).
- [30] Y. Kayanuma and N. Saito, Solid State Communications, **84**(7), 771 (1992).